Abdominal Radiology

Published online: 16 October 2018

Abdom Radiol (2019) 44:923–935
https://doi.org/10.1007/s00261-018-1800-0

Evaluation of hepatocellular carcinoma ablative margins using fused pre- and post-ablation hepatobiliary phase images

Nobuyuki Takeyama,[1] Naruki Mizobuchi,[2] Masashi Sakaki,[3] Yu Shimozuma,[3] Jiro Munechika,[2] Atsushi Kajiwara,[3] Manabu Uchikoshi,[3] Syojiro Uozumi,[3] Yoshimitsu Ohgiya,[2] and Takehiko Gokan[2]

[1]Department of Radiology, Showa University Fujigaoka Hospital, 1-30 Fujigaoka, Aoba-ku, Yokohama-City 227-8501, Japan
[2]Department of Radiology, Showa University School of Medicine, 1-5-8 Hatanodai, Shinagawa-ku, Tokyo 142-8555, Japan
[3]Department of Gastroenterology, Showa University School of Medicine, 1-5-8 Hatanodai, Shinagawa-ku, Tokyo 142-8555, Japan

Abstract

Purpose: To retrospectively evaluate the utility of fusion images of pre- and post-ablation hepatobiliary phase (HBP) series to assess the ablation margins after radiofrequency ablation (RFA) of hepatocellular carcinomas (HCCs). Additionally, to identify factors indicative of an adequate ablation margin and predictors of local tumor progression (LTP).

Methods: Fifty-nine HCCs in 29 patients were treated by RFA and followed-up for > 1 year (mean 37.9 months). Fusion images of pre- and post-ablation HBP series were created using a non-rigid registration and manual correlation. The ablation margin appearance was classified as ablation margin + (ablation margin completely surrounding the tumor), ablation margin-zero (a partially discontinuous ablation margin without protrusion of HCC), ablation margin—(a partially discontinuous ablation margin with protrusion of HCC), and indeterminate (index tumor was not visible). The minimal ablation margin was measured, and clinical factors were examined to identify other risk factors for LTP.

Results: LTP was observed at follow-up in 12 tumors. The mean minimal ablation margin was 3.6 mm. Multivariate analysis revealed that the ablation margin status was the only significant factor ($p = 0.028$). The cumulative LTP rates (3.3%, 3.3%, and 3.3% at 1, 2, and 3 years, respectively) in 30 ablation margin + nodules were significantly lower ($p = 0.006$) than those (20.0%, 28.0%, and 32.2% at 1, 2, and 3 years, respectively) in 25 ablation margin-zero nodules.

Conclusions: Fusion images enable an early assessment of the ablation efficacy in the majority of HCCs. The ablation margin status is a significant factor for LTP.

Key words: Fusion—RFA—EOB-MRI—Hepatocellular carcinoma—Hepatobiliary phase

Percutaneous radiofrequency (RF) ablation is usually indicated as a curative therapy for early-stage hepatocellular carcinomas (HCCs) [1]. It is important to create the ablation margin surrounding the index tumor of > 3–5 mm [2, 3] because it is an independent factor for progression-free survival and overall survival [1–4].

To evaluate the ablation margin after the procedure, contrast-enhanced computed tomography (CT) has been used, comparing pre-and post-ablation CT images in a side-by-side manner [5]; however, this technique may be inaccurate due to translocation, rotation, or deformation of the liver depending on the patient's position and respiratory motion. Moreover, the ablation-induced hyperemic rim surrounding the ablation zone may mimic a residual tumor [6]. To overcome these limitations, fusion imaging of pre- and post-ablation CT images have been developed for HCCs [7–10] and liver metastases [11].

Meanwhile, several researchers have investigated post-ablation magnetic resonance imaging (MRI) in the acute phase after the procedure because it can distinguish the index tumor from the ablation margin on the same image. The feasibility of T2*-weighted imaging after administration of superparamagnetic iron oxide [12] and unenhanced T1-weighted imaging was initially reported

Correspondence to: Nobuyuki Takeyama; *email:* nobuyukitakeyama@gmail.com

[13–16]. Subsequently, the utility of gadoxetate disodium (Gd-EOB-DTPA)—enhanced MRI (EOB-MRI) was identified [17–19] because post-ablation portal venous phase and hepatobiliary phase (HBP) images revealed conspicuous differentiation of the index tumor, ablation margin, and surrounding hepatic parenchyma with hypo- or hyper-intensity, intermediate-intensity, and iso-hyperintensity [17–19]. We believed that post-ablation HBP sequences could discriminate index tumors from the ablation margin most conspicuously with the least motion artifact among multiphasic images [19]. However, Koda et al. and Takeyama et al. recently revealed that many tumors became invisible 7 and 24 h after ablation, respectively [18, 19]. They concluded that approximately 25%–49% of index tumors were not identified on HBP images after the procedure. It was expected that fusion images of the pre- and post-ablation HBP series could solve the problem because MR–MR fusion images have enabled precise treatment evaluation [20–22], and post-ablation MRI examinations have been routinely acquired at our institution no more than 3 days after the procedure in patients with HCCs [17, 21].

The aim of this study was to clarify the clinical usefulness of fusion images of pre- and post-ablation HBP series, compared with post-ablation HBP sequences, using ablation margin grading. Additionally, factors to indicate an adequate ablation margin and factors to predict local tumor progression (LTP) were evaluated on fusion imaging.

Materials and methods

Patients

Our institutional review board approved this retrospective study and the informed consent requirement was waived by all patients. A computerized database of radiology reports was searched to identify all patients who met the following criteria from July 2011 to July 2016: ''RF ablation for HCC'', '' EOB-MRI before and after ablation'', and ''patients who were followed-up for $>$ 1 year [23] ''. One hundred one HCCs in 63 patients were enrolled; however, the following were excluded: 23 HCCs in 19 patients who underwent transcatheter arterial chemoembolization (TACE) as neoadjuvant therapy prior to RF ablation and 17 HCCs in 13 patients for repeated ablations as LTP adjacent to a prior ablation zone. This resulted in data on 61 HCCs in 31 patients who underwent pre-ablation EOB-MRI and post-ablation unenhanced MRI being analyzed in this study (Fig. 1). The average largest diameter of tumors was measured during HBP on pre-ablation EOB-MRI in the arterial phase and portal venous phases. Tumor location was described according to the Couinaud segmental anatomic classification, and was divided into the following three patterns: subcapsular and subdiaphragmatic; within 3 mm of the first to third branches of the portal vein, hepatic vein, or inferior vena cava; and others. The number of lesions (single or multiple) and past therapies (surgical resection, RF ablation, or TACE in other segments), as well as underlying chronic liver disease due to alcohol, hepatitis B, hepatitis C, autoimmune hepatitis, primary biliary cirrhosis, and non-alcoholic steatohepatitis, was recorded. Clinical stage was defined according to the Child–Pugh classification, and pre-treatment stages were categorized in Child–Pugh classes A and B. The diagnosis of HCC on EOB-MRI was made for nodules showing enhancement during the arterial phase with washout during the portal venous phase [23], or nodules enhancing in the arterial phase with hypointensity during the HBP when it was difficult to determine washout [24].

The inclusion criteria for RF ablation were as follows: (a) target lesions visible on ultrasound and accessible via a percutaneous route; (b) tumors $<$ 3 cm in patients who were expected to complete treatment without surgery; (c) no portal venous thrombosis or extrahepatic metastasis; (d) prothrombin time international normalized ratio [INR] $<$ 1.7; (e) serum total bilirubin $<$ 3.0/μL; and (f) platelet count $>$ 50 $\times$ 10^3/mL.

RF ablation procedure

All RF ablation procedures were performed under local anesthesia using ultrasound guidance by experienced hepatologists. A 17-gauge cooled-tip electrode that was 15 or 20 cm long with a 2 or 3 cm-long exposed metallic tip was used with a 200 Watt generator (Cool-Tip Radiofrequency System, Covidien, Boulder, CO). The optimal electrodes were selected according to the tumor location and size. The electrode was repositioned during the procedure to create an effective ablation margin surrounding the tumor. In cases with multifocal tumors, several lesions were ablated during the same session.

Ablation was started with an initial power output of 20 or 40 W for the 2 or 3 cm active tip, respectively, and increased at a rate of 10 W/min until roll-off. When the tumor was located in the hepatic dome, an artificial pleural effusion technique was used to improve the tumor visibility.

MRI protocol

Pre-ablation EOB-MRI was performed no more than 3 months (mean 50.3 ± 24.6 days, ranging from 15 to 90 days) before ablation, and post-ablation HBP sequences were acquired no more than 3 days (mean 1.3 days) after ablation. Pre- and post-RFA MRI examinations were performed by either a 1.5-T system (Avanto or Essenza, Siemens Healthcare, Erlangen, Germany) or a 3-T system (Trio, Siemens Healthcare). Pre- and post-ablation MRI included T2-weighted, diffusion-weighted, unenhanced T1-weighted, and dynamic

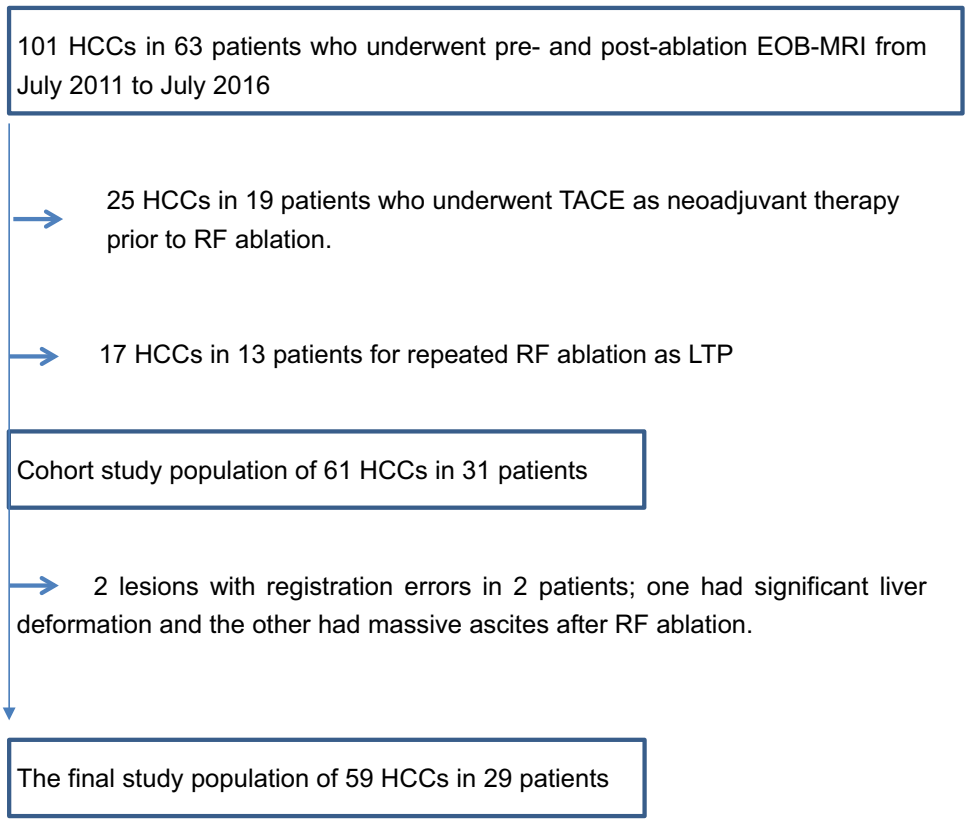

Fig. 1. Flowchart of inclusion and exclusion criteria in this study.

contrast-enhanced images with the injection of Gd-EOB-DTPA (Primovist, Bayer Healthcare, Osaka, Japan) of 0.025 mmol/kg of body weight followed by a 20 mL saline flush at a rate of 2 mL/s using a power injector. Arterial phase, portal venous phase, late phase, and HBP images were obtained at 20, 60, 120, and 20 min. Contrast-enhanced T1WI and HBP sequences were obtained with volumetric interpolated breath-hold examination (VIBE) sequences with fat saturation in the axial plane with the following parameters: TR range 2.87–4.97 ms; TE range 1.13–1.83 ms; and flip angle, 9°–15°.

The range of section thicknesses was 3.5–5.0 mm and the matrix range was from 262–420 to 379–420 pixels. The averaged section thickness was 4.0 ± 0.4 mm during pre-ablation HBP and was 4.1 ± 0.3 mm on post-ablation T1WI. The average gap between pre- and post-ablation MRI was 0.2 ± 0.3 mm, including gaps of 0 mm in 40 lesions, 0.5 mm in 17, and 1 mm in 2.

Treatment and follow-up

Patients with RF ablation for HCCs underwent unenhanced MRI or EOB-MRI examinations no more than 3 days after the procedure because the ablation margin was interpreted immediately. If hepatologists diagnosed that a tumor was not covered sufficiently by the ablation zone on post-ablation MRI, RF ablation was repeated the next day after MRI to encompass the tumor completely; however, no additional ablation was performed in this study. In all patients, after treatment efficacy was confirmed by EOB-MRI, EOB-MRI was repeated every 2–4 months for 2 years, and multiphasic contrast-enhanced CT or EOB-MRI was repeated every 6 months thereafter.

A residual tumor is defined as a tumor that is not treated during the ablation session and remains at the ablation margin. LTP was defined as a newly appearing hypervascular nodule during the arterial phase that washed out during the portal phase at the edge of an ablation zone in an area which previously showed the absence of viable tissue on at least one imaging study [25, 26]. When residual tumors or LTP were detected during the follow-up period, RF ablation or TACE was used for retreatment.

Fusion imaging

To create fused images, we used an image analyzing system (Volume Analyzer Synapse VINCENT, version 5.1, Fujifilm Medical Systems, Tokyo, Japan), which was installed in a picture archiving and communication system (PACS) (Synapse, Fujifilm Medical Systems) workstation. Our aim was to accurately fuse the Couinaud sub-segmental anatomic location around the target tu-

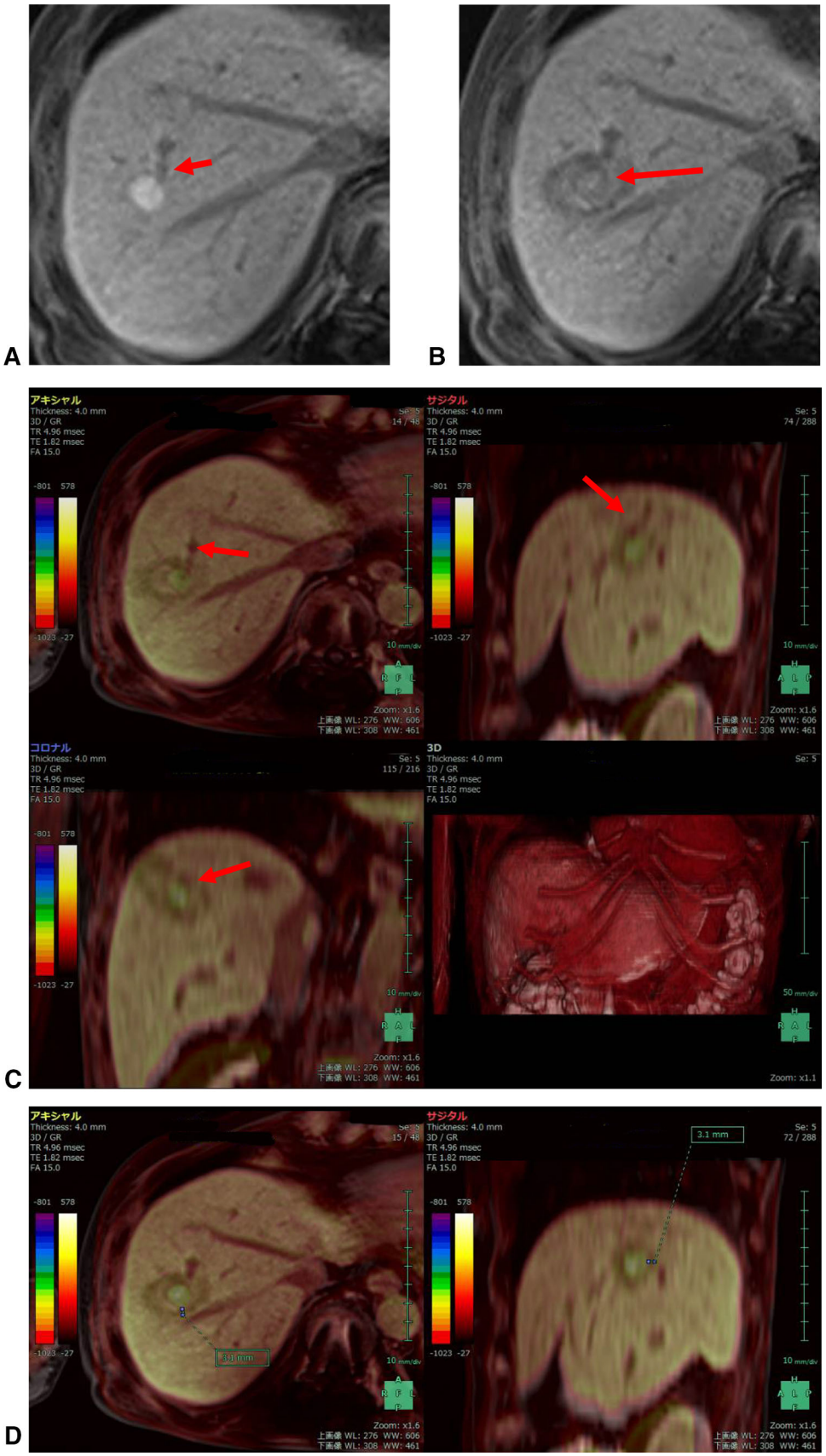
A
B
アキシャル
Thickness: 4.0 mm
3D / GR
TR 4.96 msec
TE 1.82 msec
FA 15.0
サジタル
コロナル
3D
Zoom: x1.6
C
D
3.1 mm

◀**Fig. 2.** A 55-year-old male with a 12 mm HCC abutting the third branch of the portal vein (arrowhead) at S8 of the liver. **A** Pre-ablation hepatobiliary phase image shows a hyperintense nodule abutting the third branch of the portal vein (arrow). **B** Post-ablation hepatobiliary sequence reveals an indeterminate lesion (arrow) within an intermediate-intense ablation zone. **C** Fusion imaging of pre- and post-ablation hepatobiliary phase images by screen capture demonstrated a central light green tumor circumscribed by a broad green middle zone. The status of the ablation margin was categorized as ablation margin (+). However, a residual tumor occurred at a position abutting the third branch of the portal vein (arrows) 2 months after the procedure, and transarterial chemoembolization was performed as retreatment. **D** The minimum ablation margin was 3.1 mm in the axial and sagittal views.

mor [20, 21], even if certain misregistrations occurred in other parts of the liver [3]. Image registration was repeated for lesions in other segments and lobes [3, 20].

The first step was to use the Fusion'' application, which was adapted as a rigid registration method, to superimpose pre-ablation HBP images onto post-ablation HBP sequences. The registration program was started up in the axial, coronal, sagittal and 3D views. The second step was to color target nodules and the ablation zone. When the ''fire'' color was selected among seven colors for upper images and the ''lung nodule'' color was selected from 21 colors for lower images, the index tumor and the ablation margin appeared as a reddish nodule and a yellow-green area, respectively (Fig. 2). The third step was to align the pre- and post-RFA images automatically and manually. First, automatic registration was performed referring to the signal intensity of the hepatic parenchyma. Second, manual registration was performed at the sub-segmental anatomical location around the target tumor by selecting the portal vein or hepatic venous branch around the tumor. The bifurcation point of each vessel was assigned as a landmark [7, 8]. Landmarks close to the lesion were preferably used as to fuse images accurately. Ten points in the axial view, 5 points in the coronal view, and 5 points in the sagittal view were selected because 20 points in total were available in all 3 cross-sectional views in this registration program. The fourth step was to tweak the registration image using slight shift and rotation in all views. The registration error was judged in this step. After fusion imaging was generated, it was sent to the PACS server. The mean time to create one registration image was 10–15 min.

Qualitative analysis

Two radiologists with 4 and 23 years of experience in abdominal imaging independently interpreted the post-ablation HBP sequences and fusion images using a workstation. In cases of discrepancies between the two readers, a final decision was made via consensus through reassessment with a third radiologist who had 11 years of experience in abdominal imaging. They knew the diagnosis of HCC and information about tumor location and size but were unaware of the final results with regard to whether LTP occurred during the follow-up period. They were free to use processing tools such as windowing, gradation adjustment, or magnification, and to scroll the MRI examinations. First the registration error of the branches of the portal and hepatic veins in the vicinity of the target was scored using the following 3 grading levels [8]: good, no (0 mm) vascular misregistration; fair, minimal (< 2 mm) in less than 4 vessels; and poor, minimal (< 2 mm) in more than five vessels, or severe (> 3 mm) in more than 1 vessel.

The second step was to grade the ablation margin using both post-ablation HBP sequences and fusion

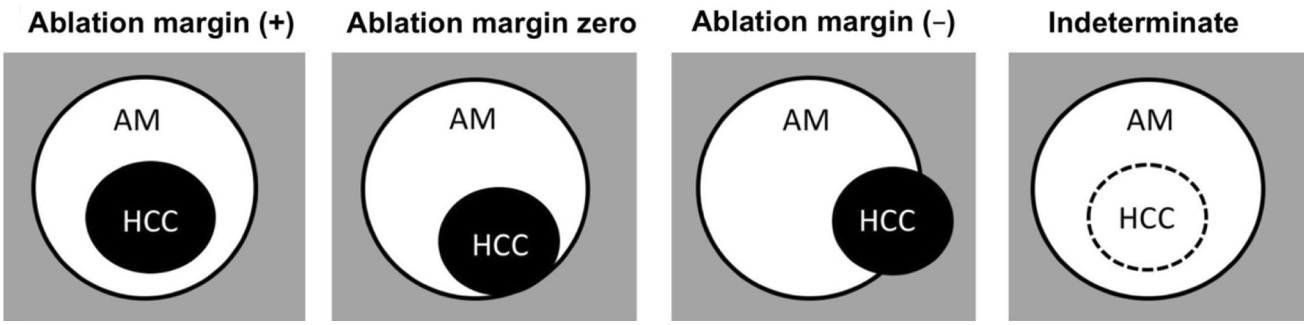

Fig. 3. Schema for the assessment of the ablation margin grading on fusion images of pre- and post-ablation hepatobiliary phase series and post-ablation hepatobiliary phase sequences: The ablation margin was categorized using 4 grades, including visible [ablation margin (+), ablation margin zero, and ablation margin (−) and indeterminate]. Visible ablation margins were classified as one of follows: ablation margin (+), in which the ablation margin completely surrounded the tumor; ablation margin zero, in which the ablation margin was partially discontinuous, without protrusion of the tumor beyond the border of the ablative margin; and ablation margin (−), in which the ablation margin was partially discontinuous, with protrusion of the tumor. A score of indeterminate was assigned when the central lesion could not be easily distinguished from the ablation margin.

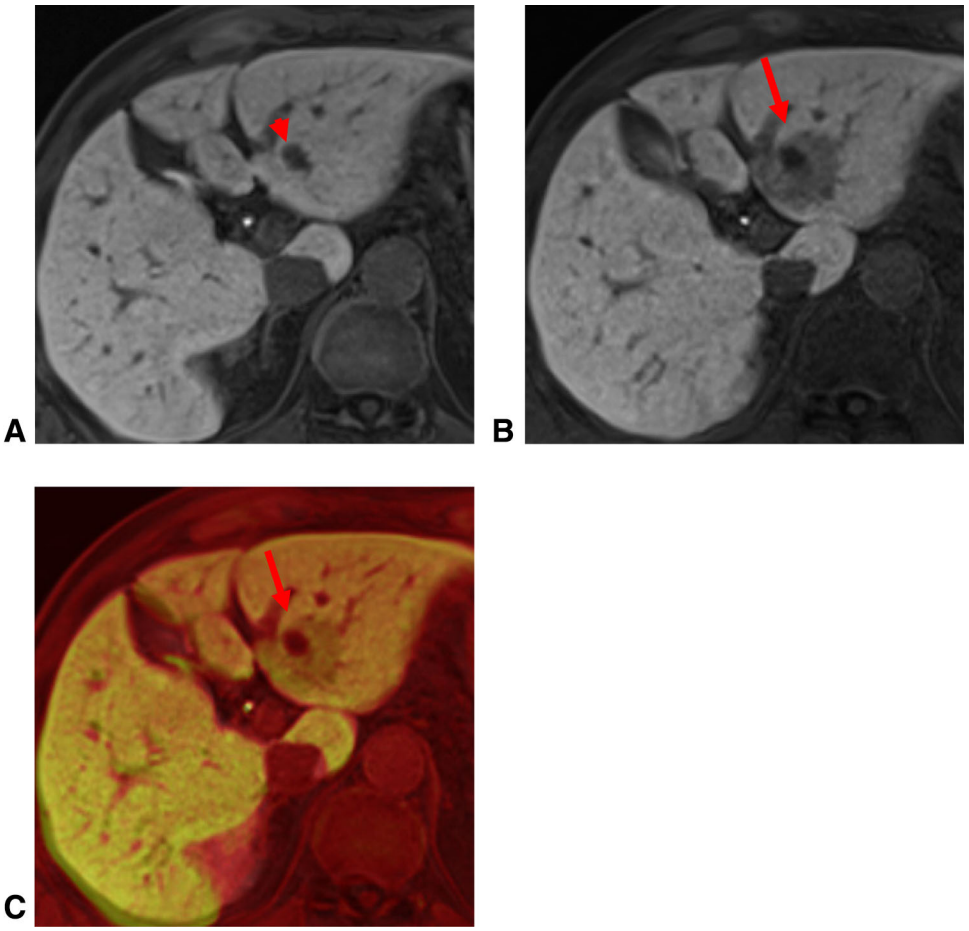

Fig. 4. A 60-year-old male with a 1.3 cm HCC in S2 of the liver. **A** Pre-ablation hepatobiliary phase image shows a hypointense nodule (arrow) 13 mm at S2. **B** Post-ablation hepatobiliary phase sequence reveals a hypointense target nodule covered by an intermediate-intense ablation margin. The ablation margin grading was evaluated as ablation margin zero, in which the ablation margin was partially discontinuous at the peripheral edge of the umbilical side (arrow). **C** Fusion image of pre- and post-ablation hepatobiliary phase series demonstrates a central reddish tumor circumscribed by a broad green middle zone (arrow). The ablation margin grading was classified as ablation margin zero. Local tumor progression occurred at this peripheral edge of the umbilical side as the ablation margin zero 12 months after the procedure, and additional ablation was performed as retreatment.

images. First, pre-ablation T1-weighted images and arterial phase, late phase and HBP images were observed, and second, post-ablation HBP sequences and fusion images were evaluated (Fig. 3). The ablation margin grading was categorized using 4 grading levels, including visible [ablation margin (+), ablation margin zero, and ablation margin (−)] and indeterminate on both post-ablation HBP sequence and fusion imaging (Fig. 4). An indeterminate ablation margin was assigned when the central lesion could not be easily distinguished from the ablation zone [15]. The ablation margin plus [ablation margin (+)] score meant the ablation zone completely surrounded the tumor. The ablation margin zero score was for a partially discontinuous ablation margin without protrusion of the tumor beyond the border of the ablative zone. The ablation margin minus [ablation margin (−)] was a partially discontinuous ablation margin with protrusion of the tumor [12, 15].

On post-ablation HBP sequences, a visible ablation margin was defined as a central hypo- or hyperintense tumor circumscribed by a hyperintense broad middle zone with a hypointense marginal band. On fusion imaging, a visible ablation margin was defined as a central red tumor circumscribed by a broad green middle zone (Fig. 5).

Quantitative analysis

The minimum ablation margin was defined as the shortest distance between the boundaries of the tumor and the periphery of the ablation margin among axial, coronal, and sagittal images on fusion imaging. In the ablation margin (+) nodules, the minimum ablation margin was measured (Figs. 2, 5). In the ablation margin zero nodules, the ablation margin was not measured (Figs. 6, 7).

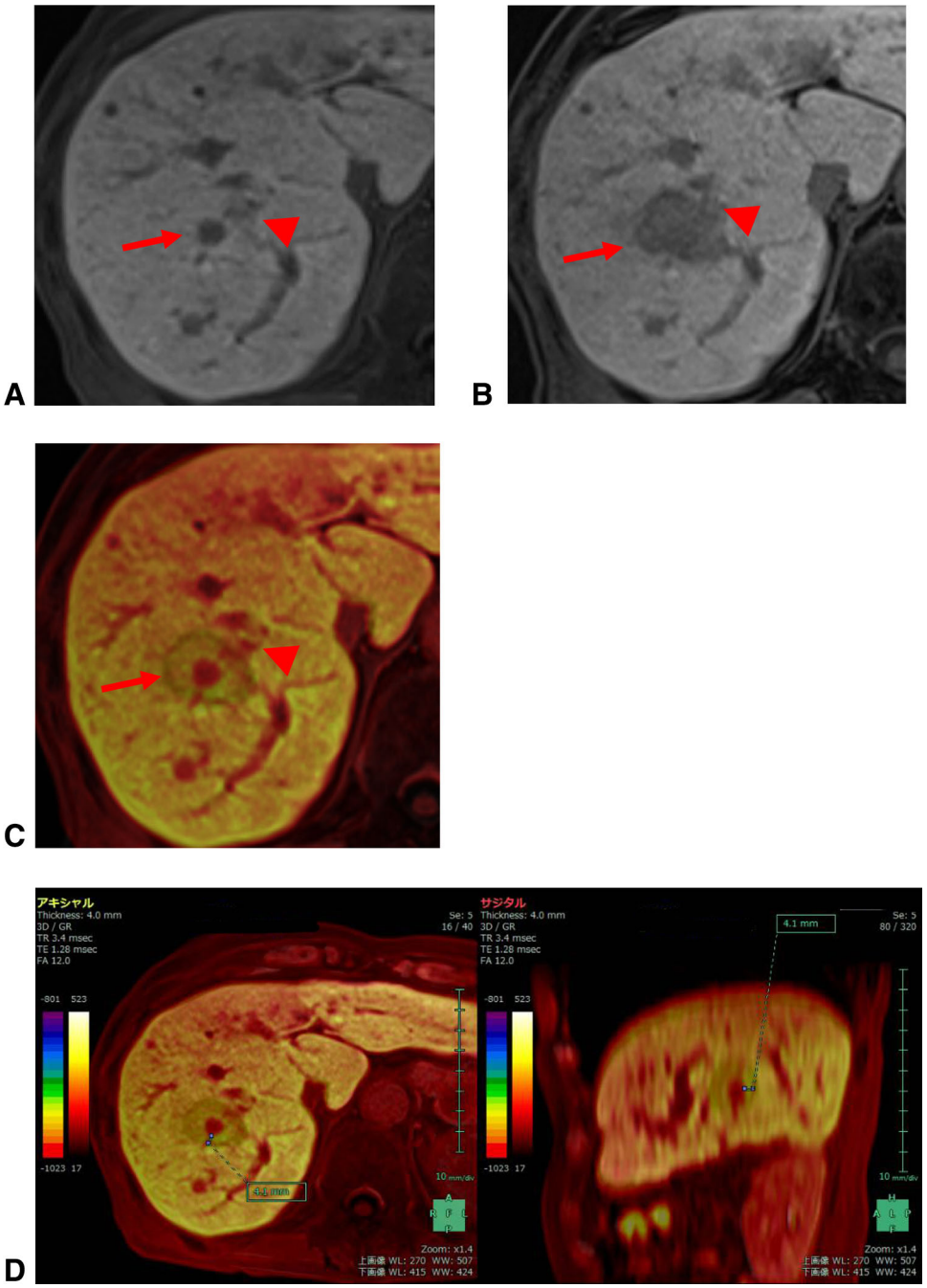

Fig. 5. A 71-year-old male with a 1 cm and 1.5 cm HCC in S8/7 of the liver. **A** Pre-ablation hepatobiliary phase image shows a 1 cm hypointense oval nodule (arrow) and a 1.5 cm heterogeneously hypointense irregular nodule (arrowhead). **B** Post-ablation HBP sequence demonstrates that both target tumors were indeterminate within the ablation zone (arrow and arrowhead). **C** Fusion image of pre- and post-ablation hepatobiliary phase series could distinguish reddish target tumors from the green ablation margin. The oval nodule (arrow) was assessed as ablation margin (+), and there was no evidence of tumor progression during 42-months' follow-up. The irregular tumor (arrowhead) was judged as ablation margin (−), and tumor progression occurred 10 months after the procedure. **D** The minimum ablation margin of the 1 cm oval nodule was 4.1 mm in the axial and sagittal views.

Statistical analysis

All data are shown as mean values ± standard deviations. Statistical analysis was performed using SPSS version 20 (IBM SPSS, Chicago, IL).

Inter-observer agreement regarding registration errors in 61 HCCs on fusion imaging was investigated using the Cohen k coefficient. Inter-observer agreement on the ablation margin grading on post-ablation HBP

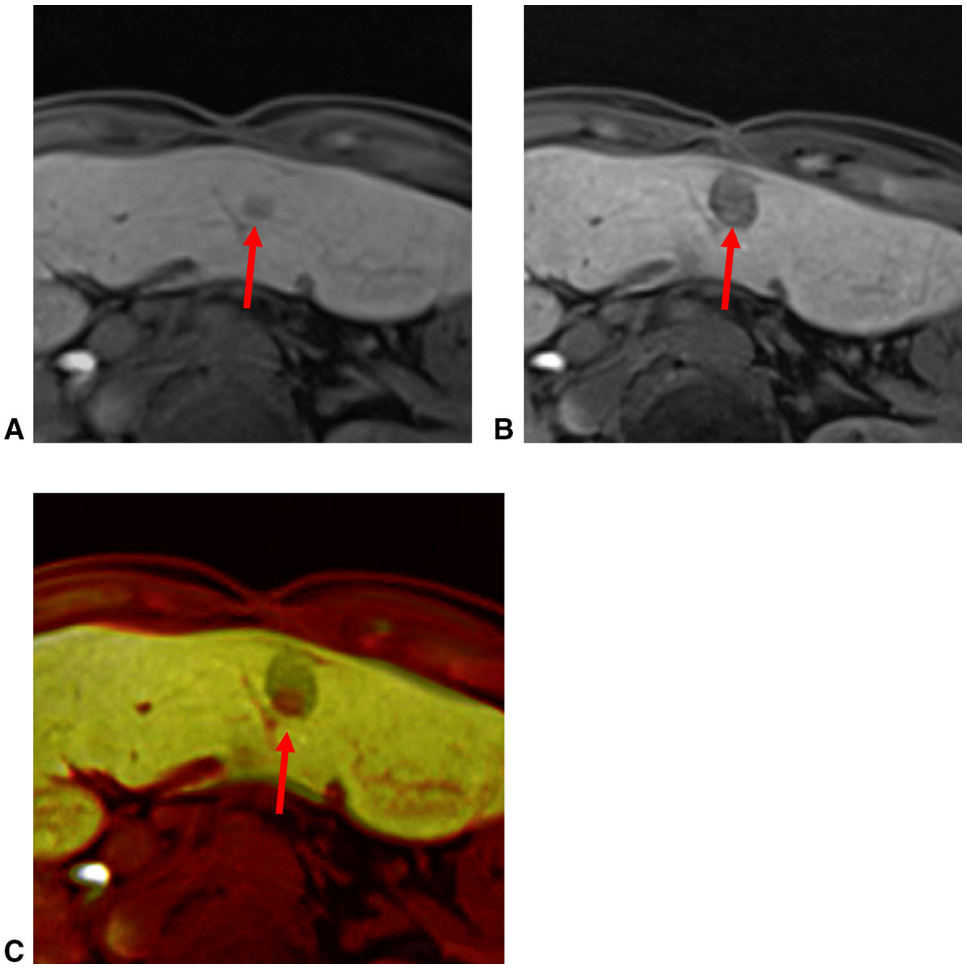

Fig. 6. A 62-year-old male with 7 mm HCC at S3 of the liver. **A** Pre-ablation hepatobiliary phase image shows a 7 mm hypointense nodule (arrow) at S3. **B** Post-ablation hepatobiliary phase sequence demonstrates an invisible index tumor within an intermediate-intense ablation zone (arrow), and the ablation margin status was classified as indeterminate. **C** Fusion imaging of pre- and post-ablation hepatobiliary phase series demonstrates a central reddish tumor circumscribed by a broad green middle zone (arrow). The ablation margin status is classified as ablation margin zero. Local tumor progression did not occur during a 36 months' follow-up period.

sequence and fusion imaging in 61 HCCs was analyzed using the Cohen k coefficient. The k values were interpreted as poor for k less than 0.20; fair, k of 0.21–0.40; moderate, k of 0.40–0.60; good, k of 0.61–0.80; and very good, k of 0.81–1.00. The numbers and percentages of patients evaluated as the ablation margin grading [ablation margin (+), ablation margin zero, ablation margin (−), and indeterminate] on post-ablation HBP sequence and fusion imaging were compared using the χ^2 test.

To compare the baseline characteristics between ablation margin (+) and ablation margin zero HCCs on fusion imaging, categorical variables were analyzed using the χ^2 test as the univariate analysis. The cumulative LTP rate was calculated using the Kaplan–Meier method and the log-rank test was used for statistical analysis (Fig. 8). A logistic regression model was used for multivariate analysis of independent factors for the ablation margin (+) on fusion imaging. The Cox proportional hazard model was used for multivariate analysis of independent factors for LTP after RF ablation. Probability values < 0.05 were considered significant.

Results

Table 1 summarizes the baseline characteristics in 29 patients with 59 HCCs.

The size and shape of the central lesions on fusion imaging and post-ablation HBP sequences were similar or slightly collapsed compared with the tumors on pre-ablation HBP images.

Assessment of ablation margin grading on fusion imaging

The assessment of registration errors for 61 HCCs on fusion imaging showed good ($n = 53$), fair ($n = 6$), and

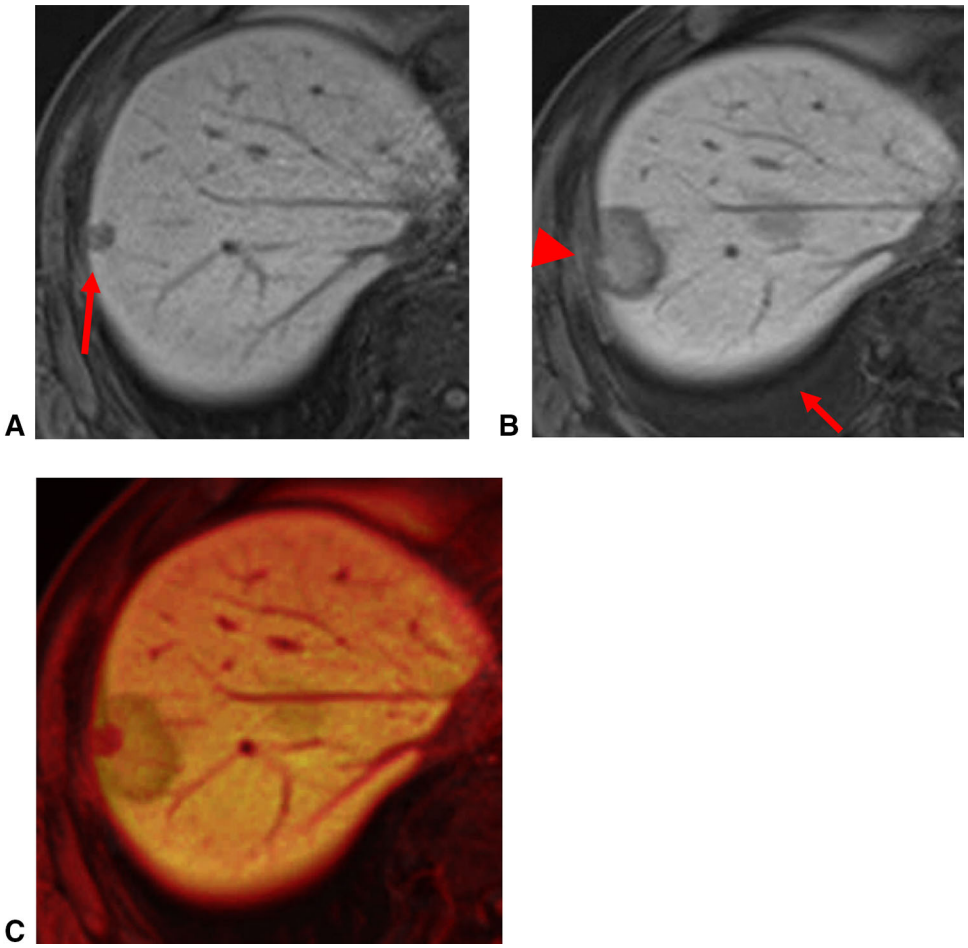

Fig. 7. A 64-year-old male with a 10-mm subcapsular HCC at S8 of the liver. **A** Pre-ablation hepatobiliary phase image shows (arrow) a hypointense nodule at S8. **B** Post-ablation hepatobiliary phase sequence depicts an invisible index tumor within an intermediate-intense ablation zone. The ablation margin status was indeterminate. Note the artificial pleural effusion (arrow) at the right thoracic base and slight capsular retraction (arrowhead) of the liver. **C** Fusion imaging of pre- and post-ablation hepatobiliary phase series demonstrates a central reddish tumor circumscribed by a broad green middle zone. The ablation margin status was classified as ablation margin zero. Local tumor progression occurred at the upper peripheral edge of the ablation zone 7 months after the procedure, and transarterial chemoembolization was performed as retreatment.

Table 1. Characteristics of 59 HCCs in 29 patients

	Value
Age (year): mean ± SD (range)	69.7 ± 8.1 (40–83)
Gender: male/female	23/6
Etiology: alcoholism/HBV/HCV/NASH	9/5/15/0
Child–Pugh score: A/B/C	53/6/0
Past history: RFA/TACE/hepatectomy/no	21/10/5/19
Follow-up (months): mean ± SD (range)	37.9 ± 12.4 (12–67)
Tumor size (mm): mean ± SD (range)	11.2 ± 4.4 (5–24)
Tumor multiplicity: simple/multiple	28/29
Tumor location	
Abutting vessels/subcapsular or diaphragmatic/no	18/25/16
Caudate lobe/left lobe/right anterior segment/ right posterior segment	2/18/21/18

HBV, hepatitis B virus; HCV, hepatitis C virus; NASH, non-alcoholic steatohepatitis; PBC, primary biliary cirrhosis; AIH, autoimmune hepatitis

poor ($n = 2$) results. The inter-observer agreement level between two radiologists for registration errors in 61 HCCs on fusion imaging was very good ($k = 0.686$).

Two HCCs with poor results were excluded due to liver deformation and massive ascites (Fig. 1). An artificial pleural effusion was used in 15 (25.4%) of 59 HCCs; however, no lesions showed registration errors.

The assessment of the ablation margin for 59 nodules revealed 58 visible ablation margin and one indeterminate ablation margin. One indeterminate ablation margin nodule, which showed isointensity on a pre-ablation HBP image, had a central light green nodule that could not be distinguished from the green ablation zone.

During the follow-up period, one residual tumor and 11 LTP occurred in 12 of 59 (20.3%), including one of 30 (3.2%) ablation margin (+) nodules, 8 of 25 (32%) ablation margin zero nodules, and 3 of 3 (100%) ablation

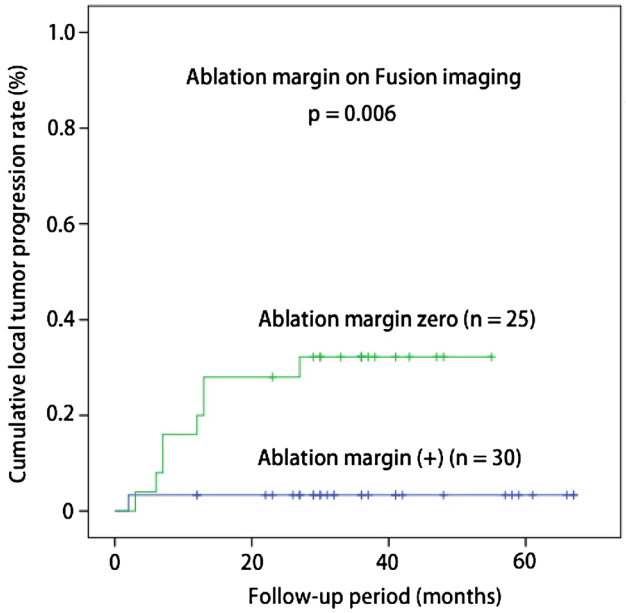

Fig. 8. The Kaplan–Meier curves according to ablation margin grading on fusion imaging. Cumulative local recurrence rates in nodules on fusion imaging of pre- and post-ablation hepatobiliary phase series: the graph shows cumulative local recurrence rates in all 55 hepatocellular carcinomas according to classification of ablative margins as follows: ablation margin zero (green line), with no residuals but sites of no margin; ablation margin (+) (blue line), which had an ablative margin with complete ablation. The log-rank test was used to calculate the *p* value.

margin (−) nodules. The remaining 47 lesions (79.7%) had no recurrence. No residual tumor or LTP was observed in the one indeterminate ablation margin nodule. The mean time to one residual tumor and 11 LTP was 10.4 ± 6.6 months, ranging from 2 to 27 months.

No case had seeding metastases at the track lines of ablation needles in this study.

Comparison of the assessment of the ablation margin grading on fusion imaging with post-ablation HBP sequences

The ablation margin grading of 59 HCCs on post-ablation HBP sequences revealed 5 ablation margin (+), 8 ablation margin (−), one ablation margin (−), and 45 indeterminate ablation margin, and that on fusion images showed 30 ablation margin (+), 25 ablation margin zero, 3 ablation margin (−) and one indeterminate ablation margin.

The inter-observer agreement level between two radiologists for the ablation margin grading on HBP sequences was very good ($k = 0.734$), and that on fusion imaging was also very good ($k = 0.693$).

A total of 14 (23.7%) out of 59 nodules were identified on post-ablation HBP sequences (Fig. 6), and 58 of 59 (98.3%) nodules were visible on fusion images. The χ^2 test (Table 2) demonstrated a significant increase ($p = 0.024$) from HBP sequences (5, 8, 1, and 45) to fusion imaging [30, 25, 3, and 1 in ablation margin (+), ablation margin zero, ablation margin (−), and indeterminate ablation margin].

The minimum ablation margin between the index tumor and the periphery of the ablation margin was 3.6 ± 0.9 mm, ranging from 1.4 to 5.6 mm, in 30 ablation margin (+) nodules.

Comparison between ablation margin (+) and ablation margin zero nodules on fusion imaging

Three ablation margin (−) and one indeterminate HCCs were excluded; therefore, baseline characteristics of 30 ablation margin (+) and 25 ablation margin zero HCCs were compared in Table 3. To evaluate the significant factors contributing to the ablation margin (+) on fusion imaging, age, gender, etiology, Child–Pugh score, past therapy, tumor size, multiplicity, and location were included in a multivariate logistic regression model. No independent factor was identified for the ablation margin (+) on fusion imaging.

During the follow-up period (median 37.9 months, range 12–67 months), the cumulative rates of LTP were significantly lower ($p = 0.006$) in the 30 ablation margin (+) nodules (3.3% at 1 years, 3.3% at 2 years, and 3.3% at 3 years) (20.0%, 28.0%, and 32.2% at 1, 2, and 3 years, respectively) in 25 ablation margin zero nodules.

Table 4 lists the clinical factors for LTP. Univariate analysis showed that the ablation margin grade was a

Table 2. Comparison of the ablation margin score between post-ablation HBP sequences and fusion images of pre- and post-ablation HBP series

Ablation margin grading	Fused images of pre- and post-ablation HBP series				Total
	Ablation margin (+)	Ablation margin-zero	Ablation margin (−)	Indeterminate	
Post-ablation HBP sequences					
AM (+)	5	0	0	0	5
AM zero	1	7	0	0	8
AM (−)	0	0	1	0	1
Indeterminate	24	18	2	1	45
Total	30	25	3	1	59

AM, ablation margin; HBP, hepatobiliary phase
K value; $p = 0.024$

Table 3. Baseline characteristics of ablation margin (+) nodules and ablation margin-zero nodules, and multivariate analysis of factors associated with ablation margin (+) on fusion images

	AM (+) (n = 30)	AM zero (n = 25)	Univariate*	Multivariate**
Age: ≥ 70 years or < 70 years	12/18	16/9	0.079	0.080
Gender: male or female	25/5	20/5	0.750	0.457
Etiology: HCV or not	16/14	15/10	0.620	0.620
Child–Pugh score: A or not	27/3	22/3	0.813	0.813
Past therapy: yes/no	19/11	17/8	0.717	0.717
Tumor size: ≥ 15/< 15 mm	24/6	23/2	0.209	0.223
Tumor multiplicity: simple/multiple	13/17	13/12	0.522	0.522
Tumor location				
Continuous vessel or not	10/20	8/17	0.916	0.638
Subcapsular or non-subcapsular	15/15	10/15	0.458	1.000
S4/8 or not	5/25	4/21	0.947	0.947

*χ^2 square test, **multivariate logistic regression analysis

Table 4. Univariate and multivariate analysis of local tumor progression after RFA in 30 ablation margin (+) and 25 ablation margin-zero nodules

Characteristics	Total (n = 55)	Local tumor progression (n = 9)	No local tumor progression (n = 46)	Univariate*	Multivariate**
Age: ≥ 70 years or < 70 years	28/27	7/2	21/25	0.084	0.108
Gender: male or female	45/10	8/1	37/9	0.578	0.585
Etiology: HCV or not	31/24	3/6	28/18	0.141	0.160
Child–Pugh score: A or not	49/6	8/1	41/5	0.958	0.958
Past therapy: yes/no	36/19	4/5	37/11	0.146	0.163
Tumor size: ≥ 15/< 15 mm	8/47	2/7	6/40	0.547	0.618
Tumor multiplicity: simple/multiple	26/29	5/4	21/25	0.556	0.570
Tumor location					
Continuous vessel or not	18/37	3/6	15/31	0.955	0.398
Subcapsular or non-subcapsular	25/30	3/6	22/24	0.433	0.501
S4/8 or not	9/46	3/6	6/40	0.090	0.495
Ablation margin status: ablation margin (+) or ablation margin-zero	30/25	1/8	29/17	0.006	0.028

significant risk factor for LTP using the log-rank test. Only ablation margin was identified as an independent factor for local tumors in a multivariate Cox proportional hazards model (Table 4).

Discussion

Post-treatment imaging is crucial to evaluate the therapy response by assessing residual and recurrent disease, revising the prognosis, and guiding further therapy [26]. The imaging sign of treatment success is a lack of vascular enhancement of the index tumor on CT or MRI examinations [5, 6]. Dynamic phases from the arterial phase to the portal venous phase plus T2-weighted images are crucial to evaluate residual tumors and LTP after ablation [27]. However, in the early post-ablation period, the peripheral rim enhancement surrounding the ablation zone may hide the local recurrence of HCCs [6, 8]. In this situation, careful comparison of pre- and post-ablation imaging with subsequent follow-up is needed to distinguish the anticipated periablation change and the tumor. Post-ablation HBP sequences do not show peripheral hyperemia, theoretically enabling us to distinguish the index tumor from the ablation margin; however, many index tumors are no longer visible after the procedure. In our study, fusion imaging was significantly superior to HBP sequences about in terms of tumor visibility within the ablation zone.

To date, various risk factors related to LTP after RF ablation have been identified. Among them are tumor diameter, the ablation margin, the minimum ablation margin, and location relative to abutting vessels and liver surface. The ablation zone is considered to be a coagulation necrosis with circumferential sinusoidal congestion and fibrosis surrounding the index tumor. The ablation margin has been recognized as the most important risk factor for LTP because it can be measured quantitatively on fusion imaging of pre- and post-ablation CT and MR. The mean ablation margin was 3.6 mm in this study; these data were in agreement within previous studies indicating a safety margin of 3–5 mm to be crucial [2, 3, 9, 10, 28]. The LTP rate of this study (3.3% at 2 and 3 years) in the ablation margin (+) nodules was similar to that in Nakazawa's research (3.5% at 3 years for HCC with an ablation margin of > 5 mm) [2] and Kudo's report (2.6% at 2 years for HCC with an ablation margin

of > 5 mm) [29]. This result suggests that the accuracy of the ablation margin grading on fusion imaging may correspond with that on enhanced CT images.

To create fusion images, a rigid registration technique was used in much the same way as the previous reports on CT–CT fusion [7, 8] and MR–MR fusion images [20]. In this registration software, segmentation of the tumor by manually tracing its contour was not performed. Only two images were overlapped when the coloring of the upper and lower images was selected to distinguish the target tumor from the ablation zone. Consequently, tumors could be clearly discriminated from the ablation zone as their size and shape were similar compared with the tumor on pre-ablation HBP images.

Despite different MR scanners and different acquisition parameters including TR, TE, FOV, and section thickness on pre- and post-ablation series, no significant registration errors were identified visually with good inter-observer agreement.

On post-ablation HBP sequences, tumor invisibility within the ablation zone could have resulted from the increased signal and shrinkage when hemorrhage and coagulation necrosis completely replaced the ablation zone [15]. We scored 76.3% of nodules as indeterminate, higher than previous reports [17–19]. We speculated that several factors may affect tumor visibility such as tumor size and signal, ablation procedure time, background liver function, and section thickness. In contrast, 98.3% of visible target lesions within the ablation zone on fusion imaging was superior to that of previous MRI studies [18, 20].

From our data, we propose a workflow to assess the ablation margin grading on fusion imaging. An ablation margin (+) has been almost completely treated because 29 of 30 (96.7%) ablation margin (+) nodules showed no residual tumor or LTP, except for one nodule abutting the third branch of the intrahepatic portal vein (Fig. 2). We found that the multivariate analysis demonstrated that ablation margin status was an independent predictor for LTP after RF ablation, as previous studies mentioned [30]. Thus, the assessment of the ablation margin on fusion images of the pre- and post-ablation HBP series can predict LTP after RF ablation. Consequently, the early and accurate detection may allow the prompt re-ablation and can improve the efficacy of the procedure [11]. It is recommended that nodules assessed as ablation margin (−) should be re-treated with the additional ablation to obtain an adequate ablation margin, HCCs evaluated as ablation zero should be carefully observed during the follow-up period and indeterminate ablation margin lesions should be evaluated again in a side-by-side manner.

There are several limitations in the present study. First, it was retrospective. Therefore, further studies are required in a prospective trial. Second, the pathology was not confirmed. Considering pathology-radiology correlation on the post-ablation unenhanced T1-weight images and post-ablation hepatobiliary phase sequences, a red tumor covered by a broad green middle zone was pathologically assumed to be the index tumor and coagulation necrosis with a peripheral inflammatory reaction [18, 19, 31]. In this study, the coagulation necrosis and peripheral inflammatory reaction were not divided and we only dealt with the ablation zone. Moreover, the histological grade of HCCs was not identified. Because poorly-differentiated HCCs could have a lower tumor-liver contrast ratio than well-differentiated HCCs [32, 33], the tumor visibility may have been affected by fusion imaging. Third, the spatial resolution of 3D-VIBE images was lower than previous reports [17–21]. Therefore, thin section thickness must employ spatial resolution on sagittal and coronal images.

In conclusion, fusion imaging of pre- and post-ablation HBP series was superior to post-ablation HBP sequences and offers the possibility of predicting the LTP using ablation margin grading. When ablation margin status is classified into ablation margin zero or ablation margin (−) on fusion imaging, additional sessions of RF ablation may be considered during the follow-up period.

Compliance with ethical standards

Funding No funding was received for this study.

Conflict of interest The authors declare that they have no conflict of interest.

Ethical approval All procedures performed in studies involving human participants were in accordance with the ethical standards of the institutional and/or national research committee and with the 1964 Helsinki Declaration and its later amendments or comparable ethical standards.

Informed consent The Institutional Review Board waived the requirement for informed consent for this retrospective study.

References

1. Shiina S, Tateishi R, Arano T, et al. (2012) Radiofrequency ablation for hepatocellular carcinoma: 10-year outcome and prognostic factors. Am J Gastroenterol 107:569–577
2. Nakazawa T, Kokubu S, Shibuya A, et al. (2007) Radiofrequency ablation of hepatocellular carcinoma: correlation between local tumor progression after ablation and ablative margin. AJR Am J Roentgenol 188:480–488
3. Kim YS, Lee WJ, Rhim H, et al. (2010) The minimal ablative margin of radiofrequency ablation of hepatocellular carcinoma (> 2 and < 5 cm) needed to prevent local tumor progression: 3D quantitative assessment. AJR Am J Roentgenol 195:758–765
4. Kei SK, Rim H, Choi D, et al. (2008) Local tumor progression after radiofrequency ablation of liver tumors: analysis of morphologic pattern and site of recurrence. AJR Am J Roentgenol 190:1544–1551
5. M-h Park, Rhim H, Kim YS, et al. (2008) Spectrum of CT findings after radiofrequency ablation of hepatic tumors. RadioGraphics 28:379–392
6. Minami Y, Nishida N, Kudo M (2014) Therapeutic response assessment of RFA for HCC: Contrast-enhanced US, CT and MRI. World J Gastroenterol 21:4160–4166
7. Tomonari A, Tsuji K, Yamazaki H, et al. (2013) Feasibility of fused imaging for the evaluation of radiofrequency ablative margin for hepatocellular carcinoma. Hepatol Res 43:728–734

8. Makino Y, Imai Y, Igura T, et al. (2013) Utility of computed tomography fusion imaging for the evaluation of the ablative margin of radiofrequency ablation for hepatocellular carcinoma and the correlation to local tumor progression. Hepatol Res 43:950–958
9. Kim KW, Lee JM, Klotz E, et al. (2011) Safety margin assessment after radiofrequency ablation of the liver using registration of preprocedure and postprocedure CT images. AJR Am J Roentgenol 196:W565–W572
10. Shin S, Lee JM, Kim KY, et al. (2014) Postablation assessment using follow-up registration of CT images before and after Radiofrequency Ablation (RFA): prospective evaluation of mid-term therapeutic results of RFA for Hepatocellular Carcinoma. AJR Am J Roentgenol 203:70–77
11. Vandenbroucke F, Vandemeulebroucke J, Buls N, Thoeni RF, de Mey J (2018) Can tumor coverage evaluated 24 h post-radiofrequency ablation predict local tumor progression of liver metastases? Int J Comput Assist Radiol Surg. https://doi.org/10.1007/s11548-018-1765-z
12. Mori K, Fukuda K, Asaoka H, et al. (2009) Radiofrequency ablation of the liver: determination of ablative margin at MR imaging with impaired clearance of ferucarbotran-feasibility study. Radiology 251:557–565
13. Onishi H, Matsushita M, Murakami T, et al. (2004) MR appearances of radiofrequency thermal ablation region: histopathologic correlation with dog liver models and an autopsy case. Acad Radiol 11:1180–1189
14. Khankan A, Murakami T, Onishi H, et al. (2008) Hepatocellular carcinoma treated with radiofrequency ablation: an early evaluation with magnetic resonance imaging. J Magn Reson Imaging 27:546–551
15. Koda M, Tokunaga S, Miyoshi K, et al. (2012) Assessment of ablative margin by unenhanced magnetic resonance imaging after radiofrequency ablation for hepatocellular carcinoma. Eur J Radiol 81:2730–2736
16. Kim SM, Shin SS, Lee BC, et al. (2017) Imaging evaluation of ablative margin and index tumor immediately after radiofrequency ablation for hepatocellular carcinoma: comparison between multi-detector-row CT and MR imaging. Abdom Radiol 42:2527–2537
17. Yoon JH, Lee EJ, Cha SS, et al. (2010) Comparison of gadoxetic acid-enhanced MR imaging versus four-phase multi-detector row computed tomography in assessing tumor regression after radiofrequency ablation in subjects with hepatocellular carcinomas. J Vasc Interv Radiol 21:348–356
18. Koda M, Tokunaga S, Okamoto T, et al. (2015) Clinical usefulness of the ablative margin assessed bymagnetic resonance imaging with Gd-EOB-DTPA for radiofrequency ablation of hepatocellular carcinoma. J Hepatol 63:1360–1367
19. Takeyama N, Vidhyarkorn S, Chung DJ, et al. (2016) Does hepatobiliary phase sequence qualitatively outperform unenhanced T1-weighted imaging in assessment of the ablation margin 24 hours after thermal ablation of hepatocellular carcinomas? Abdom Radiol 41:1942–1955
20. Makino Y, Imai Y, Igura T, et al. (2015) Comparative evaluation of three-dimensional Gd-EOB-DTPA-enhanced MR fusion imaging with CT fusion imaging in the assessment of treatment effect of radiofrequency ablation of hepatocellular carcinoma. Abdom Imaging 40:102–111
21. Sakakibara M, Ohkawa K, Katayama K, et al. (2015) Three-dimensional registration of images obtained before and after radiofrequency ablation of hepatocellular carcinoma to assess treatment adequacy. AJR Am J Roentgenol 202:W487–W495
22. Wang XL, Li K, Su ZZ, et al. (2015) Assessment of radiofrequency ablation margin by MRI-MRI image fusion in hepatocellular carcinoma. World J Gastroenterol 21:5345–5351
23. Boas FE, Do B, Louie JD (2015) Optimal imaging surveillance schedules after liver-directed therapy for hepatocellular carcinoma. J Vasc Interv Radiol 26:69–73
24. The Japan Society of Hepatology. Clinical practice guidelines for hepatocellular carcinoma, 2013. http://www.jsh.or.jp/English/guidelines_en/Guidelines_for_hepatocellular_carcinoma_2013>.r Study Group of Japan
25. Kubo M, Matsui O, Sakamoto M, et al. (2013) Role of gadolinium-ethoxybenzyl-diethylenetriamine pentaacetic acid-enhanced magnetic resonance imaging in the management of hepatocellular carcinoma: consensus at the Symposium of the 48th Annual Meeting of the Liver Cancer. Oncology 84(suppl 1):21–27
26. Lee SR, Kilcoyne A, Kambadakone A, Arellano R (2016) Interventional Oncology: pictorial review of post-ablation imaging of liver and renal tumor. Abdom Radiol 41:677–705
27. Dromain C, De Baere T, Elias D, et al. (2002) Hepatic tumors treated with percutaneous radio-frequency ablation: CT and MR imaging follow-up. Radiology 223:255–262
28. Liu CH, Arellano RS, Uppot RN, et al. (2010) Radiofrequency ablation of hepatic tumours: effect of post-ablation margin on local tumour progression. Eur Radiol 20:877–885
29. Kudo M (2004) Local ablation therapy for hepatocellular carcinoma: current status and future perspectives. J Gastroenterol 39:205–214
30. Koda M, Tokunaga S, Miyoshi K, et al. (2013) Ablative margin states by magnetic resonance imaging with ferucarbotran in radiofrequency ablation for hepatocellular carcinoma can predict local tumor progression. J Gastroenterol 48:1283–1292
31. Kim YS, Rim H, Lim HK, et al. (2011) Coagulation necrosis induced by radiofrequency ablation in the liver: histopathologic and radiologic review of usual to extremely rare changes. Radiographics 31:377–390
32. Higaki A, Ito K, Tamada T, et al. (2014) Prognosis of small hepatocellular nodules detected only at the hepatobiliary phase of Gd-EOB-DTPA-enhanced MR imaging as hypointensity in cirrhosis or chronic hepatitis. Eur Radiol 24:2476–2481
33. Chang WC, Chen RC, Chou CT, et al. (2014) Histological grade of hepatocellular carcinoma correlates with arterial enhancement on gadoxetic acid-enhanced and diffusion-weighted MR images. Abdom Imaging 39:1202–1212